Electronic Supporting Information

Unprecedented stability enhancement of multiple charged anion through decoration with negative electron affinity noble gases

Meenakshi Joshi[a,b] and Tapan K. Ghanty[a,b,*]

[a]Theoretical Chemistry Section, Chemistry Group, Bhabha Atomic Research Centre, Mumbai 400085, India.

[b]Homi Bhabha National Institute, Training School Complex, Anushakti Nagar, Mumbai–400094, India.

Computational Details

In the present work, all the calculations are performed using Turbomole 7.2 program.[1] The $B_{12}Ng_nF_{12}{}^{2-}$ (n = 1, 2, 3, 4 and 12) systems are optimized using dispersion corrected[2] DFT (B3LYP−D3)[3] and MP2[4] methods. For all the atoms def2−TZVPP basis set is used along with 28−electron core ECP for Xe atom.[5] Frequency calculation is performed with B3LYP−D3 functional to obtain minimum energy structure. Charge distribution analysis is performed using natural population analysis (NPA) scheme.[6] Furthermore, to analyze the nature of chemical bond we, have performed the atoms−in−molecule (AIM) analysis[7] and electron localization function (ELF)[7c] analysis at B3LYP−D3/def2−TZVPP level employed with energy density function (EDF)[8] using Multiwfn program[9]. For $B_{12}Ng_nF_{12}{}^{2-}$, the dissociation energy (DE) has been calculated using B3LYP−D3 and MP2 methods. In addition to this the DE has been calculated by using DLPNO−CCSD(T) method[10] with def2−TZVPP[5a] basis set and def2−TZVPP/C[11a] auxiliary basis set as implemented in ORCA4.1.2 program.[11b] Moreover, energy decomposition analysis in conjunction with the natural orbital for chemical valence (EDA−NOCV)[12] has been performed with ADF2017 software[13a,13b] using B3LYP−D3 functional and TZ2P[13c] basis set on the B3LYP−D3/def2−TZVPP optimized geometry. Scalar relativistic effect[14] has been included in the EDA−NOCV calculations. In the EDA the total interaction energy (E^{int}) between the interacting fragments is decomposed into four energy terms: the Pauli repulsion (E^{Pauli}) between the occupied orbitals of the three fragments, the classical electrostatic attractive energy (E^{elstat}) between the interacting fragments, the attractive orbital interaction energy (E^{orb}) arising from the charge transfer and mixing of the occupied and unoccupied orbitals on the fragments and the polarization effect, and the dispersion energy (E^{disp}). Moreover, in EDA−NOCV, total deformation density ($\Delta\rho(r)$) is decomposed into its individual differential densities ($\Delta\rho_i(r)$), ($\Delta\rho(r) = \sum\Delta\rho_i(r)$) which can be represented in the pairs of NOCV. The NOCV pairs of deformation density give the direction of the charge density flow. Similarly, the total E^{orb} is decomposed into its individual ΔE_i^{orb} ($E^{orb} = \sum\Delta E_i^{orb}$) corresponding to each charge transfer channel.

References

1. TURBOMOLE is program package developed by the Quantum Chemistry Group at the University of Karlsruhe, Germany, 1988: Ahlrichs, R.; Bär, M.; Häser, M.; Horn, H.; Kölmel, C. *Chem. Phys. Lett.* **1989**, *162*, 165−169.

2. a) S. Grimme, J. Antony, S. Ehrlich, H. A Krieg, *J. Chem. Phys*. **2010**, *132*, 154104. b) S. Grimme, A. Hansen, J. G. Brandenburg, C. Bannwarth, *Chem. Rev.* **2016**, *116*, 5105−5154.

3. a) A. D. Becke, *J. Chem. Phys.* **1993**, *98*, 1372−1377. b) C. Lee, W. Yang, R. G. Parr, *Phys. Rev. B* **1988***, 37*, 785−789. c) A. D. Becke, *Phys. Rev. A* **1988**, *38*, 3098−3100. d) C. Adamo, V. Barone, *J. Chem. Phys.* **1999**, *110*, 6158.

4. M. J. Frisch, M. Head−Gordon, J. A. Pople, *Chem. Phys. Lett.* **1990**, *166*, 275−280.

5. a) F. Weigenda, R. Ahlrichs, *Phys. Chem. Chem. Phys.* **2005**, *7*, 3297−3305. b) A. Schäfer, C. Huber, R. Ahlrichs, *J. Chem. Phys.* **1994**, *100*, 5829. c) K. A. Peterson, D. Figgen, E. Goll, H. Stoll, M. Dolg, *J. Chem. Phys.* **2003**, *119*, 11113.

6. A. E. Reed, R. B. Weinstock, F. A. Weinhold, *J. Chem. Phys*. **1985**, *83*, 735

7. a) R. F. W. Bader, Atoms in Molecules−A Quantum Theory; *Oxford University Press: Oxford, U.K.,* **1990**. b) W. Zou, D. Nori−Shargh, Boggs, *J. Phys. Chem. A* **2013**, *117*, 207−212. c) A. D. Becke and K. E. Edgecombe, *J. Chem. Phys.* 1990, **92**, 5397.

8. T. A. Keith, M. J. Frisch, *J. Phys. Chem. A.* **2011**, *115*, 12879−12894.

9. T. Lu, F. W. Chen, *J. Comput. Chem.* **2012**, *33*, 580−592.

10. (a) Riplinger, B. Sandhoefer, A. Hansen and F. Neese, J. Chem. Phys., 2013, 139, 134101. (b) C. Riplinger, P. Pinski, U. Becker, E. F. Valeev and F. Neese, J. Chem. Phys., 2016, 144, 024109. (c) D. G. Liakos, F. Neese, *J. Chem. Theory Comput.* **2015**, *11*, 4054−4063.

11. (a) A. Hellweg, C. Hattig, S. Hofener and W. Klopper, *Theor. Chem. Acc.* **2007**, *117*, 587. (b) F. Neese, F. Wennmohs, U. Becker, D. Bykov, D. Ganyushin, A. Hansen, R. Izsaηk, D. G. Liakos, C. Kollmar, S. Kossmann, D. A. Pantazis, ORCA, version 4.1.2; Max Planck Institute for Chemical Energy Conversion: Mülheim/Ruhr, Germany, 2014.

12. (a) T. Ziegler and A. Rauk, *Theor. Chim. Acta,* **1977**, 46, 1−10. b) M. P. Mitoraj, A. Michalak, T. A. Ziegler, *J. Chem. Theory Comput.* **2009**, *5*, 962−975. c) M. P. Mitoraj, A. Michalak, *Organometallics* **2007**, *26*, 6576−6580.

13. a) ADF2017; SCM, Theoretical Chemistry, Vrije Universiteit: Amsterdam, The Netherlands. http://www.scm.com. b) G. te Velde, F. M. Bickelhaupt, S. A. van

Gisbergen, C. Fonseca Guerra, E. J. Baerends, J. G. Snijders, T. Ziegler, *J. Comput. Chem.* **2001**, *22*, 931−967. c) E. van Lenthe, E. J. Baerends, *J. Comput. Chem.* **2003**, *24*, 1142–1156.

14. a) E. van Lenthe, E. J. Baerends, J. G. Snijders, *J. Chem. Phys.* **1994**, *101*, 9783–9792. b) E. van Lenthe, A. E. Ehlers, E. J. Baerends, *J. Chem. Phys.* **1999**, *110*, 8943–8953.

List of Tables

Table S1. Binding Energy of First and Second Excess Electrons ($\Delta E1$ and $\Delta E2$, in eV) in $B_{12}F_{12}^{2-}$ and $B_{12}Ng_nF_{12}^{2-}$ (Ng = Kr−Xe and n = 1, 2, 3, 4 and 12) at B3LYP−D3/Def2−TZVPP Level of Theory.

Table S2. Optimized Ng−B and Ng−F Bond Distances (in Å) in $B_{12}Ng_nF_{12}^{2-}$ (Ng = Ar−Xe and n = 1, 2, 3, 4 and 12) using B3LYP−D3 and MP2 Methods and Dissociation Energy (DE, kcal mol^{-1}) using B3LYP−D3 (B3), MP2 and DLPNO−CCSD(T)[a] Methods with def2−TZVPP Basis Set. Covalent Ng−B and Ng−F Radii[b] Reported by Cordero et al[c] [Pyykkö[d]] are also Provided in the Table.

Table S3. Calculated NPA Charge on Ng, B and F atoms in $B_{12}F_{12}^{2-}$ and $B_{12}Ng_nF_{12}^{2-}$ (Ng = Ar-Xe and n = 1, 2, 3, 4 and 12) at B3LYP−D3/def2−TZVPP Level of Theory.

Table S4. Free Energy Change (ΔG, kcal mol^{-1}) of $B_{12}Ng_nF_{12}^{2-}$ (Ng = Ar−Xe and n = 1, 2, 3, 4, 12) at 298.15 K along Path1 and Path2 Dissociation channels at B3LYP−D3/def2−TZVPP Level of Theory.

Table S5: Calculated Values of Dissociation Energy (DE, in kcal mol^{-1}) and Free energy of Dissociation (ΔG at 298.15 K, in kcal mol^{-1}) of $B_{12}Ng_nF_{12}^{2-}$ (Ng = Ar, Kr, Xe and n = 1, 2, 3, 4, 12) along Path3 and Path4 using B3LYP-D3/def2-TZVPP Method.

Table S6: Calculated Values of Optimized Bond Length (in Å), B1-Ng-F Bond Angle (in Degree) and Activation Energy Barrier (AE, in kcal mol^{-1}) of Transition State Structure (along B1-Ng-F mode) of $B_{12}Ng_nF_{12}^{2-}$ (Ng = Kr, Xe and n = 1, 2, 3, 4, 12) using B3LYP-D3/def2-TZVPP Method.

Table S7. Bond Critical Point (BCP) Properties of Ng−B (Ng−F) Bond of $B_{12}Ng_nF_{12}^{2-}$ (Ng = Kr−Xe and n = 1, 12) Compounds at B3LYP−D3/def2−TZVPP Level of Theory. BCP Properties of Ng−F Bond are Reported in the Parenthesis.

Table S8. EDA−NOCV of $B_{12}Ng_nF_{12}^{2-}$ (Ng = Kr−Xe and n = 1, 12) Along Path1 and Path2 at B3LYP−D3/TZ2P Level of Theory. The Percent Contribution of Stabilizing Energy Terms ($E^{elstat} + E^{orb} + E^{disp}$) to the Total Interaction Energy (E^{int}) is provided in the parenthesis. All Energy Terms are in kcal mol^{-1}.

List of Figures

Figure S6. Scaled MOs energy level diagram of $B_{12}Xe_{12}F_{12}{}^{2-/-/0}$ using B3LYP-D3/def2-TZVPP method. The red and blue lines correspond to the alpha and beta orbitals respectively, of $B_{12}Xe_{12}F_{12}{}^{(-)}$ system. The orbital energies of the negative and neutral systems are scaled by keeping the energy of the highest occupied molecular orbitals (HOMO) of $B_{12}Xe_{12}F_{12}{}^{(-)}$ and $B_{12}Xe_{12}F_{12}$ to that of the HOMO of $B_{12}Xe_{12}F_{12}{}^{2-}$ system.

Figure S7. MOs pictures of lowest unoccupied molecular orbital (LUMO), highest occupied molecular orbital (HOMO), singly occupied molecular orbital (SOMO) and additional 10 outer valence occupied molecular orbitals of $B_{12}Kr_{12}F_{12}{}^{(2-)}$ and $B_{12}Kr_{12}F_{12}{}^{(-)}$ systems using B3LYP-D3/def2-TZVPP method.

Figure S8. MOs pictures of LUMO, HOMO, SOMO and additional 10 outer valence occupied molecular orbitals of $B_{12}Kr_{12}F_{12}{}^{(-)}$ and $B_{12}Kr_{12}F_{12}$ systems using B3LYP-D3/def2-TZVPP method.

Figure S9. MOs pictures of LUMO, HOMO, SOMO and additional 10 outer valence occupied molecular orbitals of $B_{12}Xe_{12}F_{12}{}^{(2-)}$ and $B_{12}Xe_{12}F_{12}{}^{(-)}$ systems using B3LYP-D3/def2-TZVPP method.

Figure S10. MOs pictures of LUMO, HOMO, SOMO and additional 10 outer valence occupied molecular orbitals of $B_{12}Xe_{12}F_{12}{}^{(-)}$ and $B_{12}Xe_{12}F_{12}$ systems using B3LYP-D3/def2-TZVPP method.

Figure S11. Dissociation energy (DE, kcal mol^{-1}) plot of $B_{12}Kr_nF_{12}{}^{2-}$ (n =1, 2, 3, 4, 12) along Path1 and Path2 dissociation channels using B3LYP−D3, MP2 and DLPNO−CCSD(T) methods with def2−TZVPP basis set.

Figure S12. Deformation density ($\Delta\rho$(r)) pictures of the pairwise orbital interactions for $B_{12}Kr_nF_{12}{}^{2-}$ (n = 1 and 12) along Path1 and Path2 and their associated ΔE_i^{orb} energies (ΔE^{σ} and ΔE^{π}, in kcal mol^{-1}) obtained from the EDA−NOCV at B3LYP−D3/TZ2P level of theory. The blue and red colored surfaces indicate regions with $\Delta\rho$(r) > 0 and $\Delta\rho$(r) < 0, respectively.

Figure S13. Deformation density ($\Delta\rho(r)$) pictures of the pairwise orbital interactions for $B_{12}Xe_nF_{12}{}^{2-}$ (n = 1 and 12) along Path1 and Path2 and their associated ΔE_i^{orb} energies (ΔE^σ and ΔE^π, in kcal mol^{-1}) obtained from the EDA−NOCV at B3LYP−D3/TZ2P level of theory. The blue and red colored surfaces indicate regions with $\Delta\rho(r) > 0$ and $\Delta\rho(r) < 0$, respectively.

Table S1. Binding Energy of First and Second Excess Electrons ($\Delta E1$ and $\Delta E2$, in eV) in $B_{12}F_{12}^{2-}$ and $B_{12}Ng_nF_{12}^{2-}$ (Ng = Kr−Xe and n = 1, 2, 3, 4 and 12) at B3LYP−D3/Def2−TZVPP Level of Theory

Dianions	$\Delta E1$		$\Delta E2$	
$B_{12}F_{12}^{2-}$	5.51		1.31	
	Kr	Xe	Kr	Xe
$B_{12}NgF_{12}^{2-}$	6.21	6.05	2.15	2.07
$1,12-B_{12}Ng_2F_{12}^{2-}$	6.94	6.40	2.53	2.70
$1,2,12-B_{12}Ng_3F_{12}^{2-}$	7.47	6.76	2.79	3.07
$1,2,7,12-B_{12}Ng_4F_{12}^{2-}$	7.69	7.05	3.16	3.37
$B_{12}Ng_{12}F_{12}^{2-}$	8.47	7.87	5.22	5.15

Table S2. Optimized Ng−B and Ng−F Bond Distances (in Å) in $B_{12}Ng_nF_{12}^{2-}$ (Ng = Ar−Xe and n = 1, 2, 3, 4 and 12) using B3LYP−D3 and MP2 Methods and Dissociation Energy (DE, kcal mol^{-1}) using B3LYP−D3 (B3), MP2 and DLPNO−CCSD(T)[a] Methods with def2−TZVPP Basis Set. Covalent Ng−B and Ng−F Radii[b] Reported by Cordero et al[c] [Pyykkö[d]] are also Provided in the Table

$B_{12}Ng_nF_{12}^{2-}$	Ng-B		Ng−F		DE Along PATH1			DE Along PATH2		
	B3	MP2	B3	MP2	B3	MP2	DLPNO−CCSD(T)	B3	MP2	DLPNO−CCSD(T)
$R_{cov(Ar-B)/(Ar-F)}$	1.900 [1.810]	1.900 [1.810]	1.630 [1.600]	1.630 [1.600]						
$B_{12}ArF_{12}^{2-}$	1.950	1.862	2.304	2.311	54.8	55.2	46.1	4.2	7.1	3.0
$1,7-B_{12}Ar_2F_{12}^{2-}$	1.946	1.853	2.253	2.246	46.1	45.5	36.2	13.9	21.0	7.6
$1,12-B_{12}Ar_2F_{12}^{2-}$	1.943	1.854	2.255	2.251	47.3	47.0	36.8	17.5	21.2	17.1
$1,2,12-B_{12}Ar_3F_{12}^{2-}$	1.948	1.850	2.207	2.182	35.4	34.1	24.6	23.7	32.0	28.2
$1,7,12-B_{12}Ar_3F_{12}^{2-}$	1.947	1.850	2.207	2.183	40.6	39.0	29.3	24.4	32.1	28.8
$1,2,7,12-B_{12}Ar_4F_{12}^{2-}$	1.958	1.853	2.173	2.126	...*	29.1	22.9	28.7	39.7	35.2
$B_{12}Ar_{12}F_{12}^{2-}$	2.005	...*	2.060	...*	3.0	...*	...*	61.2	...*	71.8
$R_{cov(Kr-B)/(Kr-F)}$	2.000 [2.020]	2.000 [2.020]	1.730 [1.810]	1.730 [1.810]						
$B_{12}KrF_{12}^{2-}$	2.098	2.011	2.339	2.322	64.6	67.3	57.9	14.0	19.2	14.7
$1,7-B_{12}Kr_2F_{12}^{2-}$	2.096	2.009	2.296	2.270	57.6	60.0	50.2	23.5	31.2	27.8
$1,12-B_{12}Kr_2F_{12}^{2-}$	2.094	2.009	2.297	2.274	58.4	60.6	50.4	26.3	31.8	27.6
$1,2,12-B_{12}Kr_3F_{12}^{2-}$	2.096	2.011	2.255	2.220	49.3	60.0	41.4	32.6	41.0	37.3
$1,7,12-B_{12}Kr_3F_{12}^{2-}$	2.096	2.011	2.255	2.220	53.0	55.2	44.7	33.2	41.0	37.7
$1,2,7,12-B_{12}Kr_4F_{12}^{2-}$	2.101	2.018	2.222	2.177	45.6	48.6	37.8	38.0	47.8	44.5
$B_{12}Kr_{12}F_{12}^{2-}$	2.130	2.084	2.113	2.062	25.7	35.6	19.6	72.0	77.2	81.7
$R_{cov(Xe-B)/(Xe-F)}$	2.240 [2.160]	2.240 [2.160]	1.970 [1.950]	1.970 [1.950]						
$B_{12}XeF_{12}^{2-}$	2.270	2.178	2.371	2.350	78.7	86.7	74.3	28.1	38.5	31.1
$1,7-B_{12}Xe_2F_{12}^{2-}$	2.268	2.179	2.340	2.315	73.6	81.7	69.7	36.3	48.3	41.7
$1,12-B_{12}Xe_2F_{12}^{2-}$	2.268	2.179	2.341	2.316	73.9	81.7	69.2	38.8	49.5	42.3
$1,2,12-B_{12}Xe_3F_{12}^{2-}$	2.271	2.184	2.308	2.280	67.8	76.6	63.5	43.6	56.6	49.7
$1,7,12-B_{12}Xe_3F_{12}^{2-}$	2.271	2.184	2.287	2.280	70.0	78.1	65.4	44.7	56.8	50.3
$1,2,7,12-B_{12}Xe_4F_{12}^{2-}$	2.277	2.190	2.282	2.250	65.1	74.2	60.9	49.0	62.8	56.3
$B_{12}Xe_{12}F_{12}^{2-}$	2.302	2.222	2.189	2.157	51.4	65.6	47.9	81.1	99.0	91.0

[a]Single point energy calculation is performed using DLPNO−CCSD(T) method on B3LYP−D3 optimized geometry

*Structure did not converge

[b]$R_{cov(Ng-B)} = R_{cov(Ng)} + R_{cov(B)}$ and $R_{cov(Ng-F)} = R_{cov(Ng)} + R_{cov(F)}$

[c]B. Cordero, V. Gómez,, Ana E. Platero-Prats, M. Revés, J. Echeverría, E. Cremades, F. Barragán, S. Alvarez, *Dalton Trans.* **2008**, 2832–2838. [d]P. Pyykkö, *J. Phys. Chem. A* **2015**, 119, 11, 2326-2337.

Table S3. Calculated NPA Charge on Ng, B and F atoms in $B_{12}F_{12}^{2-}$ and $B_{12}Ng_nF_{12}^{2-}$ (Ng = Ar−Xe and n = 1, 2, 3, 4, 12) at B3LYP−D3/def2−TZVPP Level of Theory

$B_{12}Ng_nF_{12}^{2-}$	$q_{tot}B$	$q_{tot}F$	q_{totB+F}	$q_{tot}Ng$	$q_{avg}B$	$q_{avg}F$	$q_{avg}Ng$
$B_{12}F_{12}^{2-}$	3.64	−5.64	−2.00	...	0.30	−0.46	...
$B_{12}ArF_{12}^{2-}$	3.37	−5.89	−2.52	0.52	−0.11	−0.88	0.52
$1,7−B_{12}Ar_2F_{12}^{2-}$	3.10	−6.16	−3.06	1.06	−0.13	−0.85	0.53
$1,12−B_{12}Ar_2F_{12}^{2-}$	3.10	−6.16	−3.06	1.07	−0.12	−0.86	0.53
$1,2,12−B_{12}Ar_3F_{12}^{2-}$	2.77	−6.40	−3.63	1.63	−0.13	−0.82	0.54
$1,7,12−B_{12}Ar_3F_{12}^{2-}$	2.77	−6.40	−3.63	1.63	−0.13	−0.82	0.54
$1,2,7,12−B_{12}Ar_4F_{12}^{2-}$	2.42	−6.60	−4.18	2.18	−0.12	−0.78	0.54
$B_{12}Ar_{12}F_{12}^{2-}$	−0.72	−7.85	−8.57	6.57	−0.06	−0.65	0.55
$B_{12}KrF_{12}^{2-}$	3.27	−5.90	−2.63	0.63	−0.21	−0.86	0.63
$1,7−B_{12}Kr_2F_{12}^{2-}$	2.90	−6.18	−3.28	1.29	−0.23	−0.84	0.64
$1,12−B_{12}Kr_2F_{12}^{2-}$	2.90	−6.19	−3.29	1.29	−0.23	−0.85	0.64
$1,2,12−B_{12}Kr_3F_{12}^{2-}$	2.47	−6.45	−3.98	1.98	−0.23	−0.82	0.66
$1,7,12−B_{12}Kr_3F_{12}^{2-}$	2.47	−6.45	−3.98	1.98	−0.23	−0.82	0.66
$1,2,7,12−B_{12}Kr_4F_{12}^{2-}$	2.03	−6.70	−4.67	2.67	−0.22	−0.80	0.67
$B_{12}Kr_{12}F_{12}^{2-}$	−1.92	−8.44	−10.36	8.36	−0.16	−0.70	0.70
$B_{12}XeF_{12}^{2-}$	3.16	−5.92	−2.76	0.76	−0.33	−0.86	0.76
$1,7−B_{12}Xe_2F_{12}^{2-}$	2.67	−6.23	−3.56	1.56	−0.34	−0.84	0.78
$1,12−B_{12}Xe_2F_{12}^{2-}$	2.66	−6.23	−3.57	1.56	−0.34	−0.84	0.78
$1,2,12−B_{12}Xe_3F_{12}^{2-}$	2.14	−6.53	−4.39	2.39	−0.33	−0.83	0.80
$1,7,12−B_{12}Xe_3F_{12}^{2-}$	2.14	−6.53	−4.39	2.39	−0.33	−0.83	0.80
$1,2,7,12−B_{12}Xe_4F_{12}^{2-}$	1.59	−6.82	−5.23	3.24	−0.31	−0.81	0.81
$B_{12}Xe_{12}F_{12}^{2-}$	−3.26	−9.03	−12.29	10.29	−0.27	−0.75	0.86

Table S4. Free Energy Change (ΔG, kcal mol^{-1}) of $B_{12}Ng_nF_{12}^{2-}$ (Ng = Ar−Xe and n = 1, 2, 3, 4, 12) at 298.15 K along Path1 and Path2 Dissociation channels at B3LYP−D3/def2−TZVPP Level of Theory.

$B_{12}Ng_nF_{12}^{2-}$	ΔG	
	Path1[a]	Path2[b]
$B_{12}ArF_{12}^{2-}$	38.0	-15.0
$1,7-B_{12}Ar_2F_{12}^{2-}$	28.9	-4.0
$1,12-B_{12}Ar_2F_{12}^{2-}$	30.3	-1.3
$1,2,12-B_{12}Ar_3F_{12}^{2-}$	17.7	5.5
$1,7,12-B_{12}Ar_3F_{12}^{2-}$	23.4	6.4
$1,2,7,12-B_{12}Ar_4F_{12}^{2-}$	*	10.5
$B_{12}Ar_{12}F_{12}^{2-}$	-21.0	40.7
$B_{12}KrF_{12}^{2-}$	47.8	-5.2
$1,7-B_{12}Kr_2F_{12}^{2-}$	40.4	5.5
$1,12-B_{12}Kr_2F_{12}^{2-}$	41.3	7.4
$1,2,12-B_{12}Kr_3F_{12}^{2-}$	31.8	14.5
$1,7,12-B_{12}Kr_3F_{12}^{2-}$	35.8	15.3
$1,2,7,12-B_{12}Kr_4F_{12}^{2-}$	28.1	20.3
$B_{12}Kr_{12}F_{12}^{2-}$	5.2	51.4
$B_{12}XeF_{12}^{2-}$	61.7	8.7
$1,7-B_{12}Xe_2F_{12}^{2-}$	56.4	18.3
$1,12-B_{12}Xe_2F_{12}^{2-}$	56.8	19.8
$1,2,12-B_{12}Xe_3F_{12}^{2-}$	50.4	25.7
$1,7,12-B_{12}Xe_3F_{12}^{2-}$	52.8	26.8
$1,2,7,12-B_{12}Xe_4F_{12}^{2-}$	47.7	31.4
$B_{12}Xe_{12}F_{12}^{2-}$	30.7	60.4

[a]Path1: $B_{12}Ng_nF_{12}^{2-}$ $Ng + F + B_{12}Ng_{n-1}F_{11}^{2-}$
[b]Path2: $B_{12}Ng_nF_{12}^{2-}$ $Ng + F + B_{12}Ng_{n-1}F_{11}^{2-}$

Table S5: Calculated Values of Dissociation Energy (DE, in kcal mol^{-1}) and Free energy of Dissociation (ΔG at 298.15 K, in kcal mol^{-1}) of $B_{12}Ng_nF_{12}^{2-}$ (Ng = Ar, Kr, Xe and n = 1, 2, 3, 4, 12) along Path3 and Path4 using B3LYP-D3/def2-TZVPP Method.

$B_{12}Ng_nF_{12}^{2-}$	Path3 $B_{12}Ng_nF_{12}^{2-} \rightarrow B_{12}F_{12}^{2-} + nNg$		Path4 $B_{12}Ng_nF_{12}^{2-} \rightarrow B_{12}Ng_{n-1}F_{12}^{2-} + Ng$	
	DE per Ng[1]	ΔG per Ng[2]	DE	ΔG
$B_{12}ArF_{12}^{2-}$	-92.67	-41.91	-92.67	-41.91
$1,12-B_{12}Ar_2F_{12}^{2-}$	-96.07	-73.67	-99.47	-105.43
$1,2,12-B_{12}Ar_3F_{12}^{2-}$	-100.41	-87.83	-109.10	-116.15
$1,7,12-B_{12}Ar_3F_{12}^{2-}$	-100.41	-87.83	-109.10	-116.14
$1,2,7,12-B_{12}Ar_4F_{12}^{2-}$	-104.25	-96.57	-115.75	-122.80
$B_{12}Ar_{12}F_{12}^{2-}$	-120.60	-122.95	-138.16	-146.39
$B_{12}KrF_{12}^{2-}$	-82.67	-32.15	-82.67	-32.15
$1,12-B_{12}Kr_2F_{12}^{2-}$	-85.47	-63.31	-88.26	-94.46
$1,2,12-B_{12}Kr_3F_{12}^{2-}$	-89.04	-76.69	-96.18	-103.47
$1,7,12-B_{12}Kr_3F_{12}^{2-}$	-89.03	-76.69	-96.17	-103.45
$1,2,7,12-B_{12}Kr_4F_{12}^{2-}$	-92.24	-84.82	-101.85	-109.23
$B_{12}Kr_{12}F_{12}^{2-}$	-105.99	-108.69	-120.51	-129.16
$B_{12}XeF_{12}^{2-}$	-68.59	-18.21	-68.59	-18.21
$1,12-B_{12}Xe_2F_{12}^{2-}$	-70.67	-48.63	-72.75	-79.04
$1,2,12-B_{12}Xe_3F_{12}^{2-}$	-73.37	-61.14	-78.79	-86.17
$1,7,12-B_{12}Xe_3F_{12}^{2-}$	-73.38	-61.15	-78.80	-86.20
$1,2,7,12-B_{12}Xe_4F_{12}^{2-}$	-75.88	-68.61	-83.40	-90.99
$B_{12}Xe_{12}F_{12}^{2-}$	-86.71	-89.68	-98.31	-107.37

[1] DE = DE^{total} /No of dissociated Ng atom, DE^{total} = E($B_{12}F_{12}^{2-}$)+n*E(Ng)-E($B_{12}Ng_nF_{12}^{2-}$)
[2] ΔG = ΔG^{total} /No of dissociated Ng atom, ΔG^{total} = G($B_{12}F_{12}^{2-}$)+n*G(Ng)-G($B_{12}Ng_nF_{12}^{2-}$)"

Table S6: Calculated Values of Optimized Bond Length (in Å), B-Ng-F Bond Angle (in Degree) and Activation Energy Barrier (AE, in kcal mol^{-1}) of Transition State Structure (along B1-Ng-F mode) of $B_{12}Ng_nF_{12}^{2-}$ (Ng = Kr, Xe and n = 1, 2, 3, 4, 12) using B3LYP-D3/def2-TZVPP Method.

TS-$B_{12}Ng_nF_{12}^{2-}$	B-Ng	Ng-F	B-Ng-F	AE
$B_{12}KrF_{12}^{2-}$	2.155	2.570	81.01	25.52
$1,12-B_{12}Kr_2F_{12}^{2-}$	2.104	2.542	85.88	24.50
$1,2,12-B_{12}Kr_3F_{12}^{2-}$	2.083	2.506	87.67	22.89
$1,2,7,12-B_{12}Kr_4F_{12}^{2-}$	2.069	2.490	91.19	22.49
$B_{12}Kr_{12}F_{12}^{2-}$	2.093	2.344	117.33	16.33
$B_{12}XeF_{12}^{2-}$	2.347	2.581	71.70	32.52
$1,12-B_{12}Xe_2F_{12}^{2-}$	2.330	2.567	70.92	31.47
$1,2,12-B_{12}Xe_3F_{12}^{2-}$	2.301	2.520	74.12	30.21
$1,2,7,12-B_{12}Xe_4F_{12}^{2-}$	2.266	2.511	83.93	29.67
$B_{12}Xe_{12}F_{12}^{2-}$	2.267	2.432	114.42	21.23

Table S7. Bond Critical Point (BCP) Properties of Ng−B (Ng−F) Bond of $B_{12}Ng_nF_{12}^{2-}$ (Ng = Kr−Xe and n = 1, 12) Compounds at B3LYP−D3/def2−TZVPP Level of Theory. BCP Properties of Ng−F Bond are Reported in the Parenthesis

$B_{12}Ng_nF_{12}^{2-}$	ρ	$\nabla^2\rho$	V(r)	$E_d(r)$	ELF
$B_{12}KrF_{12}^{2-}$	0.09 (0.05)	−0.09 (0.18)	−0.11 (−0.05)	−0.06 (0.00)	0.58 (0.14)
$B_{12}Kr_{12}F_{12}^{2-}$	0.10 (0.08)	−0.10 (0.25)	−0.08 (−0.09)	−0.05 (−0.02)	0.83 (0.25)
$B_{12}XeF_{12}^{2-}$	0.09 (0.06)	−0.10 (0.17)	−0.07 (−0.06)	−0.05 (−0.01)	0.83 (0.18)
$B_{12}Xe_{12}F_{12}^{2-}$	0.09 (0.08)	−0.08 (0.21)	−0.06 (−0.10)	−0.04 (−0.02)	0.87 (0.27)

Table S8. EDA−NOCV of $B_{12}Ng_nF_{12}{}^{2-}$ (Ng = Kr−Xe and n = 1, 12) Along Path1 and Path2 at B3LYP−D3/TZ2P Level of Theory. The Percent Contribution of Stabilizing Energy Terms ($E^{elstat} + E^{orb} + E^{disp}$) to the Total Interaction Energy (E^{int}) is provided in the parenthesis. All Energy Terms are in kcal mol^{-1}

$B_{12}Ng_nF_{12}{}^{2-}$	Path	E^{Pauli}	E^{elstat}	E^{orb}	E^{disp}	E^{def}	E^{int}
$B_{12}KrF_{12}{}^{2-}$	Path1	222.2	−124.0 (41.7)	−168.5 (56.7)	−4.6 (1.5)	0.9	−74.1
	Path2	107.9	−11.5 (9.0)	−111.6 (87.4)	−4.6 (3.6)	7.9	−12.0
$B_{12}Kr_{12}F_{12}{}^{2-}$	Path1	238.9	−113.9 (41.4)	−154.1 (56.0)	−7.3 (2.7)	0.6	−35.8
	Path2	209.9	−95.3 (33.0)	−186.4 (64.5)	−7.3 (2.5)	6.0	−73.1
$B_{12}XeF_{12}{}^{2-}$	Path1	241.8	−138.3 (42.1)	−185.1 (56.3)	−5.3 (1.6)	0.8	−86.1
	Path2	134.8	−28.8 (17.1)	−134.1 (79.7)	−5.3 (3.2)	9.1	−24.3
$B_{12}Xe_{12}F_{12}{}^{2-}$	Path1	276.0	−137.6 (41.0)	−188.0 (56.0)	−10.2 (3.0)	1.5	−58.4
	Path2	233.5	−109.6 (34.1)	−201.8 (62.7)	−10.2 (3.2)	11.1	−77.2
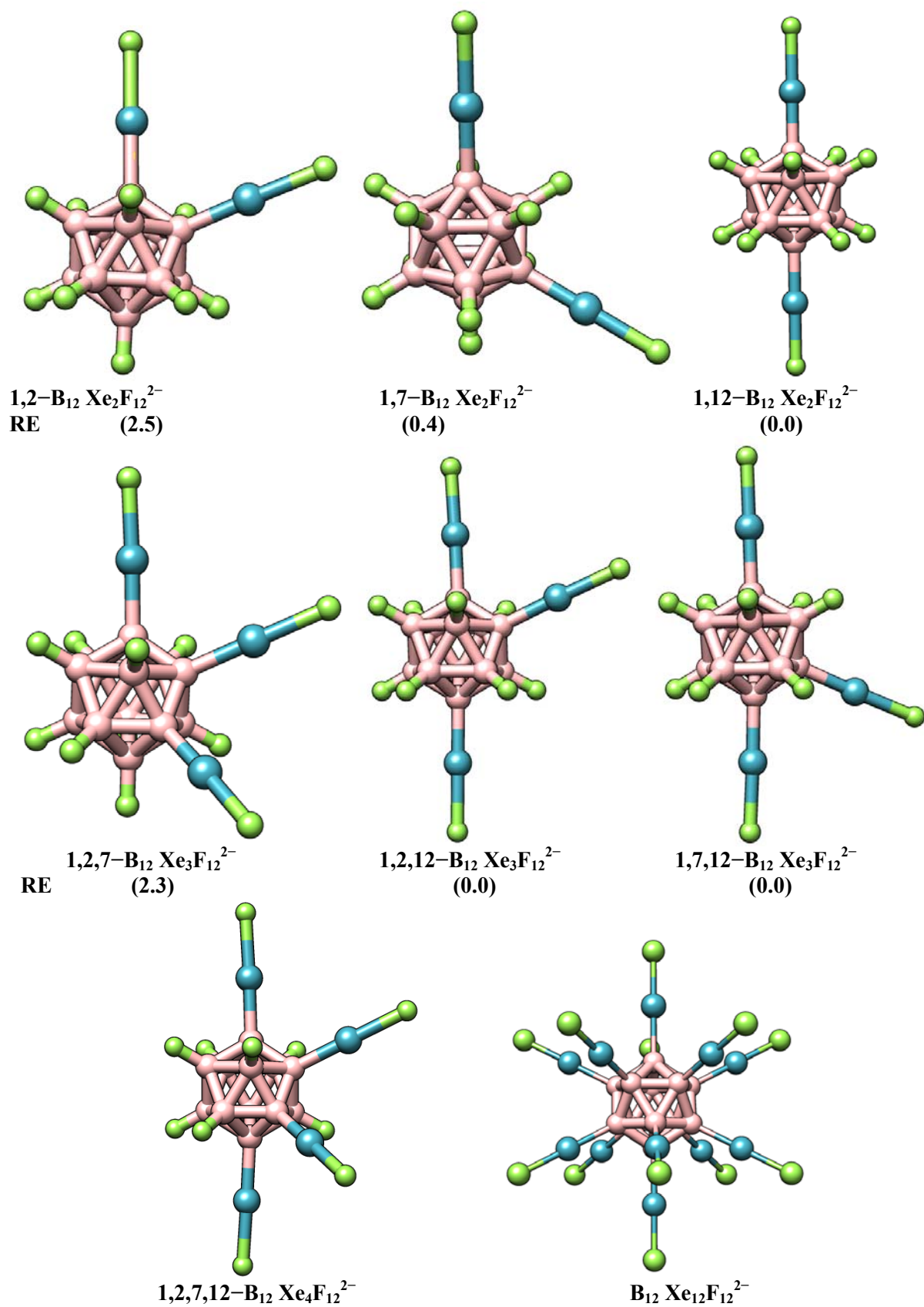
Figure S1. Optimized Structures of $B_{12}Xe_nF_{12}^{2-}$ (n = 2−4, 12) compound and relative energy (RE, in kcal mol^{-1}) of different isomers with respect to its corresponding most stable isomer.
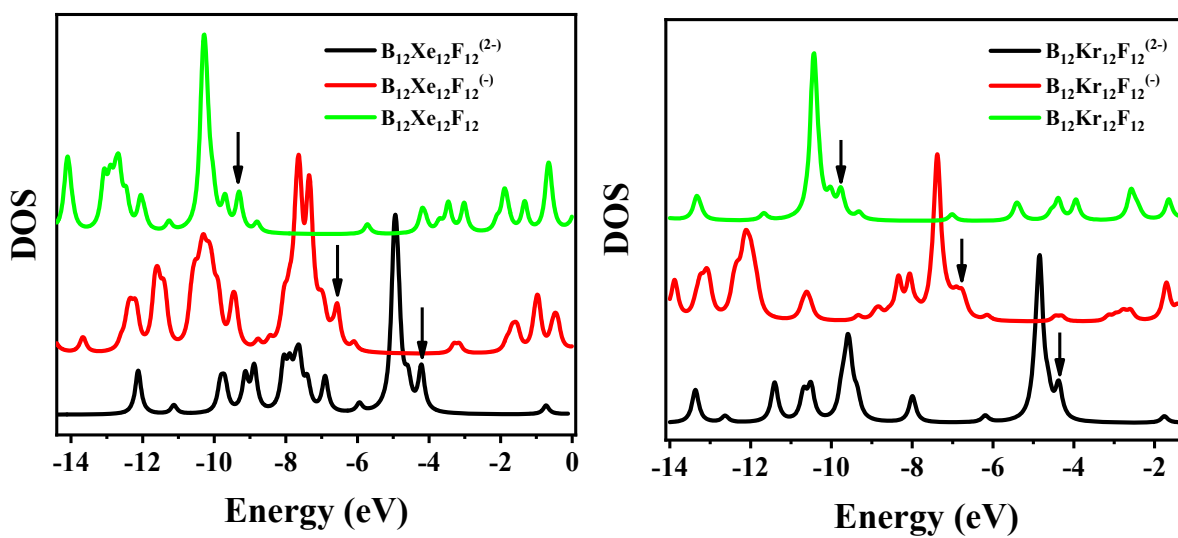
Figure S2. DOS of $B_{12}Xe_{12}F_{12}^{2-/-/0}$ and $B_{12}Kr_{12}F_{12}^{2-/-/0}$ systems using B3LYP-D3/def2-TZVPP method. Vertical arrows are pointing toward HOMO.
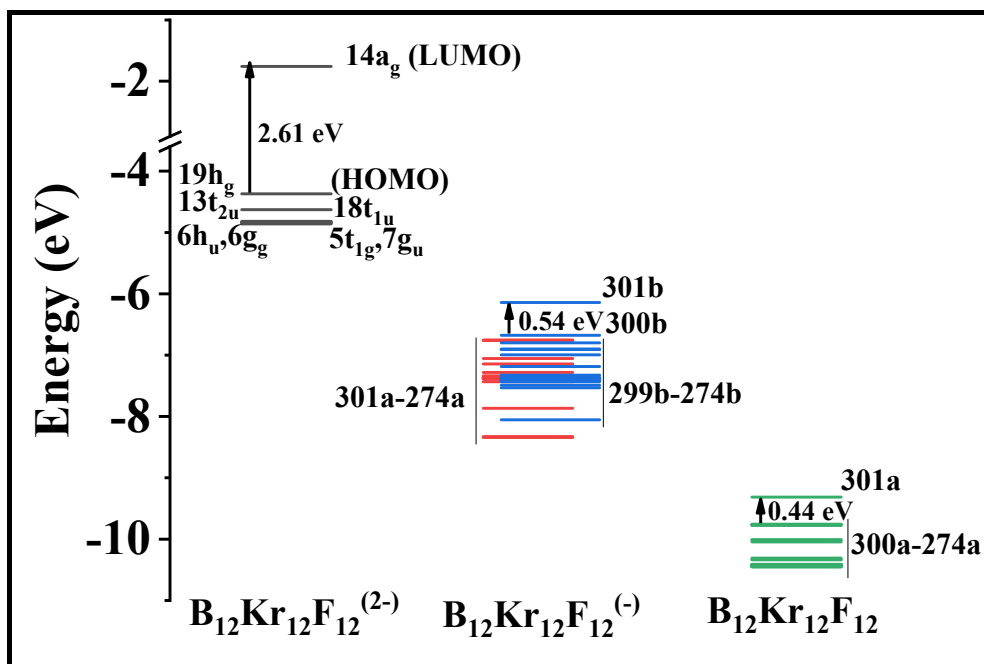
Figure S3. MOs energy level diagram of $B_{12}Kr_{12}F_{12}^{2-/-/0}$ using **B3LYP-D3/def2-TZVPP method. The red and blue lines correspond to the alpha and beta orbitals respectively, of $B_{12}Kr_{12}F_{12}^{(-)}$ system.**
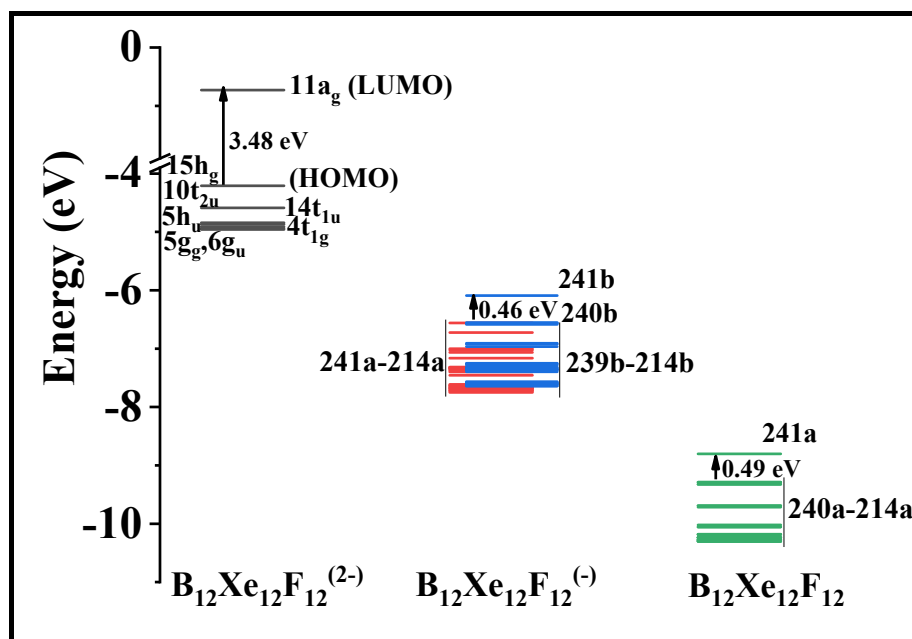
Figure S4. MOs energy level diagram of $B_{12}Xe_{12}F_{12}^{2-/-/0}$ using **B3LYP-D3/def2-TZVPP method. The red and blue lines correspond to the alpha and beta orbitals respectively, of $B_{12}Xe_{12}F_{12}^{(-)}$ system.**
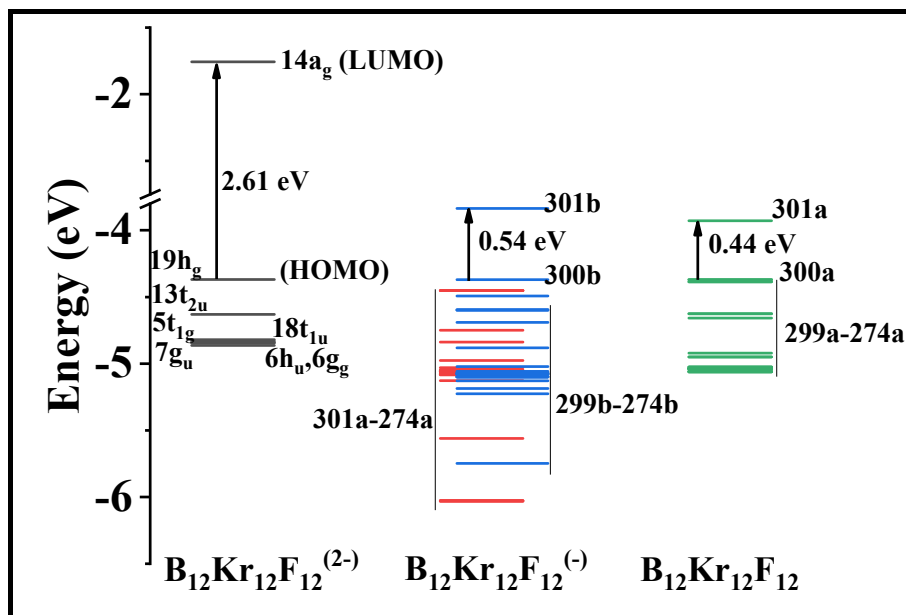
Figure S5. Scaled MOs energy level diagram of $B_{12}Kr_{12}F_{12}^{2-/-/0}$ using B3LYP-D3/def2-TZVPP method. The red and blue lines correspond to the alpha and beta orbitals respectively, of $B_{12}Kr_{12}F_{12}^{(-)}$ system. The orbital energies of the negative and neutral systems are scaled by keeping the energy of the highest occupied molecular orbitals (HOMO) of $B_{12}Kr_{12}F_{12}^{(-)}$ and $B_{12}Kr_{12}F_{12}$ to that of the HOMO of $B_{12}Kr_{12}F_{12}^{2-}$ system.

Figure S6. Scaled MOs energy level diagram of $B_{12}Xe_{12}F_{12}^{2-/-/0}$ using B3LYP-D3/def2-TZVPP method. The red and blue lines correspond to the alpha and beta orbitals respectively, of $B_{12}Xe_{12}F_{12}^{(-)}$ system. The orbital energies of the negative and neutral systems are scaled by keeping the energy of the highest occupied molecular orbitals (HOMO) of $B_{12}Xe_{12}F_{12}^{(-)}$ and $B_{12}Xe_{12}F_{12}$ to that of the HOMO of $B_{12}Xe_{12}F_{12}^{2-}$ system.

$B_{12}Kr_{12}F_{12}^{(2-)}$	$B_{12}Kr_{12}F_{12}^{(-)}$
14a_g (LUMO)	**301b (LUMO)**
[B(s)+F(p)+Kr(p)]	**[B(s,p)+F(p)+Kr(s)]**
19h_g-1 (HOMO) **19h_g-2** **19h_g-3**	**300b (HOMO)** **301a (SOMO)** **299a**
[B(s,p)+F(p)+Kr(s)]	**[B(s,p)+F(p)+Kr(s)]**
19h_g-4 **19h_g-5**	**298a** **297a** **296a**
[B(s,p)+F(p)+Kr(s)]	**[B(s,p)+F(p)+Kr(s)]**
13t_{2u}-1 **13t_{2u}-2** **13t_{2u}-3**	**295a** **294a** **293a**
[B(s)+F(p)+Kr(s)]	**[B(s,p)+F(p)+Kr(s)]** **[F(p)]** **[F(p)+Kr(p)]**
18t_{1u}-1 **18t_{1u}-2** **18t_{1u}-3**	**292a** **291a** **290a**
[B(s,p)+F(p)]	**[F(p)+Kr(p)]**

Figure S7. MOs pictures of lowest unoccupied molecular orbital (LUMO), highest occupied molecular orbital (HOMO), singly occupied molecular orbital (SOMO) and additional 10 outer valence occupied molecular orbitals of $B_{12}Kr_{12}F_{12}^{(2-)}$ and $B_{12}Kr_{12}F_{12}^{(-)}$ systems using B3LYP-D3/def2-TZVPP method.

B$_{12}$Kr$_{12}$F$_{12}$$^{(-)}$	B$_{12}$Kr$_{12}$F$_{12}$
301b (LUMO)	301a (LUMO)
[B(s,p)+F(p)+Kr(s)]	[B(s,p)+F(p)+Kr(s)]
300b (HOMO) 301a (SOMO) 299a	300a (HOMO) 299a 298a
[B(s,p)+F(p)+Kr(s)]	[B(s,p)+F(p)+Kr(s)]
298a 297a 296a	297a 296a 295a
[B(s,p)+F(p)+Kr(s)]	[B(s,p)+F(p)+Kr(s)]
295a 294a 293a	294a 293a 292a
[B(s,p)+F(p)+Kr(s)] [F(p)] [F(p)+Kr(p)]	[B(s,p)+F(p)+Kr(s)]
292a 291a 290a	291a 290a
[F(p)+Kr(p)]	[B(s,p)+F(p)+Kr(s)] [F(p)]

Figure S8. MOs pictures of LUMO, HOMO, SOMO and additional 10 outer valence occupied molecular orbitals of B$_{12}$Kr$_{12}$F$_{12}$$^{(-)}$ and B$_{12}$Kr$_{12}$F$_{12}$ systems using B3LYP-D3/def2-TZVPP method.

$B_{12}Xe_{12}F_{12}^{(2-)}$	$B_{12}Xe_{12}F_{12}^{(-)}$
11a$_g$ (LUMO)	**241b (LUMO)**
[B(s)+F(p)+Xe(p)]	**[B(s,p)+F(p)+Xe(s)]**
15h$_g$-1 (HOMO) **15h$_g$-2** **15h$_g$-3**	**240b (HOMO)** **241a (SOMO)** **239a**
[B(s,p)+F(p)+Xe(s)]	**[B(s,p)+F(p)+Xe(s)]**
15h$_g$-4 **15h$_g$-5**	**238a** **237a** **236a**
[B(s,p)+F(p)+Xe(s)]	**[B(s,p)+F(p)+Xe(s)]**
10t$_{2u}$-1 **10t$_{2u}$-2** **10t$_{2u}$-3**	**235a** **234a** **233a**
[B(s,p)+F(p)+Xe(s)]	**[F(p)+Xe(p)]**
14t$_{1u}$-1 **14t$_{1u}$-2** **14t$_{1u}$-3**	**232a** **231a** **230a**
[B(s,p)+F(p)]	**[F(p)+Xe(p)]**
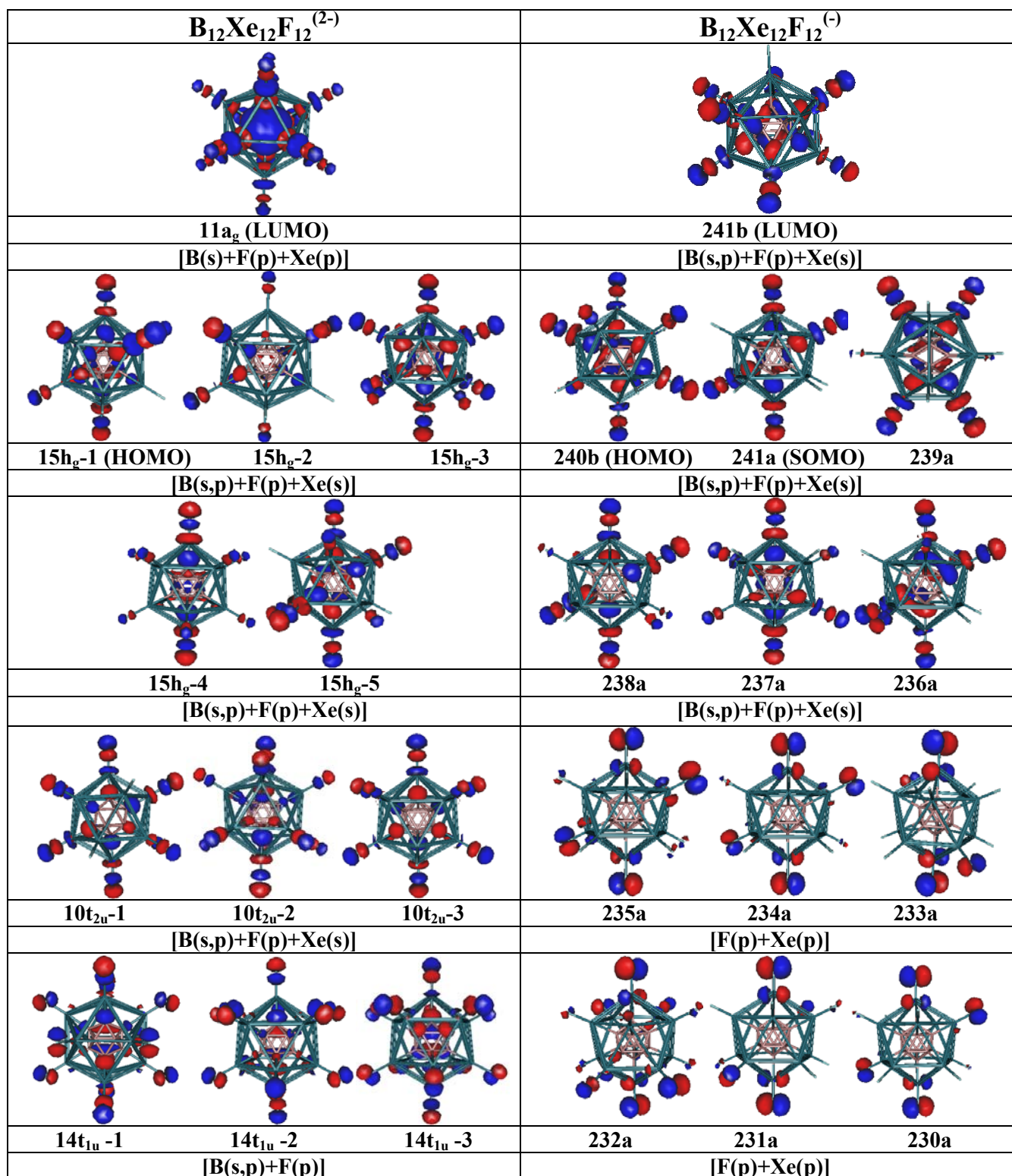
Figure S9. MOs pictures of LUMO, HOMO, SOMO and additional 10 outer valence occupied molecular orbitals of $B_{12}Xe_{12}F_{12}^{(2-)}$ and $B_{12}Xe_{12}F_{12}^{(-)}$ systems using B3LYP-D3/def2-TZVPP method.

$B_{12}Xe_{12}F_{12}^{(-)}$	$B_{12}Xe_{12}F_{12}$
241b (LUMO)	241a (LUMO)
[B(s,p)+F(p)+Xe(s)]	[B(s,p)+F(p)+Xe(s)]
240b (HOMO) 241a (SOMO) 239a	240a (HOMO) 239a 238a
[B(s,p)+F(p)+Xe(s)]	[B(s,p)+F(p)+Xe(s)]
238a 237a 236a	237a 236a 235a
[B(s,p)+F(p)+Xe(s)]	[B(s,p)+F(p)+Xe(s)]
235a 234a 233a	234a 233a 232a
[F(p)+Xe(p)]	[B(s,p)+F(p)+Xe(s)]
232a 231a 230a	231a 230a
[F(p)+Xe(p)]	[B(s,p)+F(p)+Xe(s)] [F(p)+Xe(p)]

Figure S10. MOs pictures of LUMO, HOMO, SOMO and additional 10 outer valence occupied molecular orbitals of $B_{12}Xe_{12}F_{12}^{(-)}$ and $B_{12}Xe_{12}F_{12}$ systems using B3LYP-D3/def2-TZVPP method.
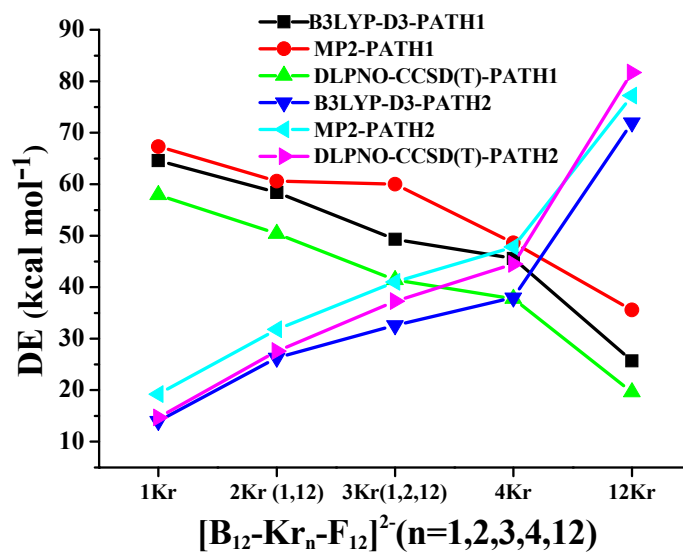
Figure S11. Dissociation energy (DE, kcal mol^{-1}) plot of $B_{12}Kr_nF_{12}^{2-}$ (n =1, 2, 3, 4, 12) along Path1 and Path2 dissociation channels using B3LYP−D3, MP2 and DLPNO−CCSD(T) methods with def2−TZVPP basis set.
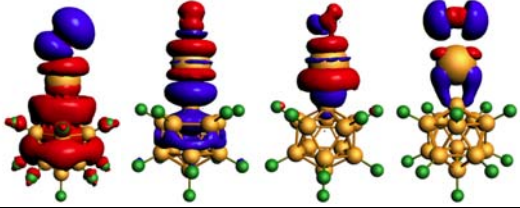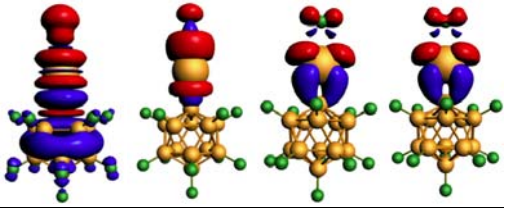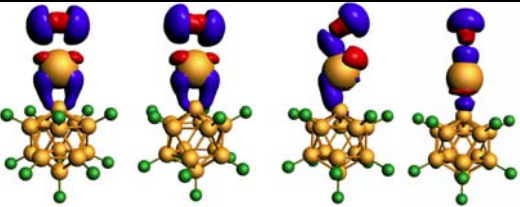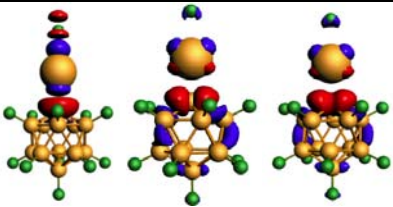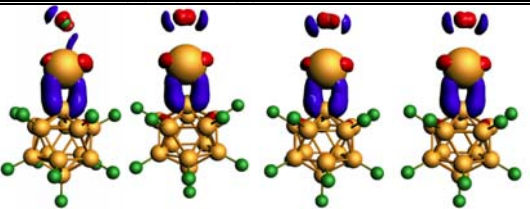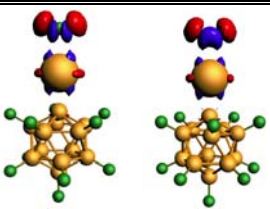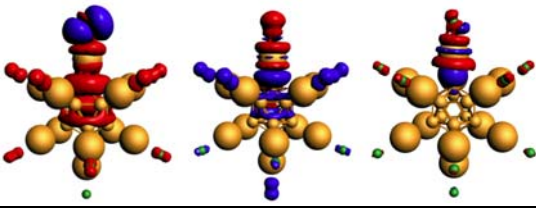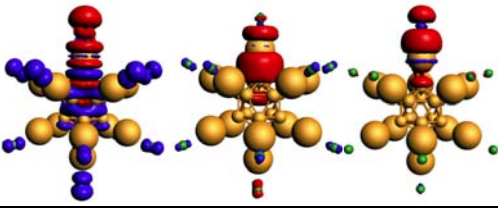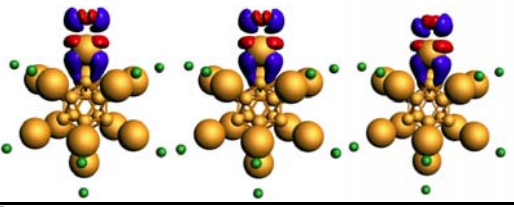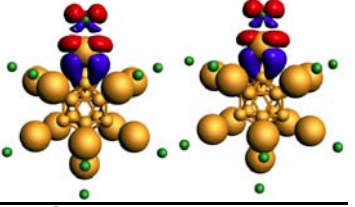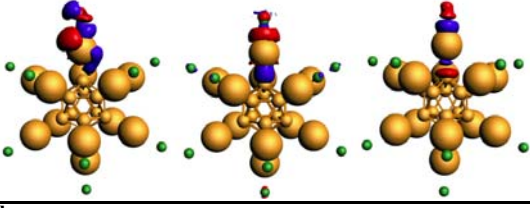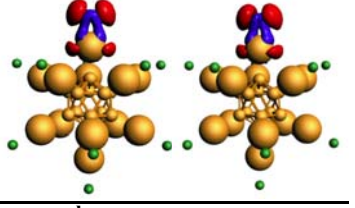
Path1 (Dianion+F+Ng) [$E^{orb} = \sum \Delta E_i^{orb}$]	Path2(Anion+F$^-$ +Ng) [$E^{orb} = \sum \Delta E_i^{orb}$]
KrB$_{12}$F$_{12}^{2-}$ (E^{orb} =−168.5)	KrB$_{12}$F$_{12}^{2-}$(E^{orb} =−111.6)

ΔE_i^{orb} =−132.9(b)   −15.3(a)   −9.5(b)   0.22(a)

ΔE_i^{orb} =−89.3   −4.4   −5.3   −5.3

ΔE_i^{orb} = −1.0(b)   0.3(a)   −1.6(b)   −0.8(a)

ΔE_i^{orb} = −3.1   −0.45   −0.45

ΔE_i^{orb} = −1.1(b) −0.7(a)   −1.0(b)   −0.5(a)

ΔE_i^{orb} = −0.19   −0.19

Kr$_{12}$B$_{12}$F$_{12}^{2-}$(E^{orb} =−154.1)	Kr$_{12}$B$_{12}$F$_{12}^{2-}$(E^{orb} =−186.4)

ΔE_i^{orb} = −88.3(b)   −31.0(a)   −13.5(b)

ΔE_i^{orb} = −146.9   −10.8   −6.4

ΔE_i^{orb} = −1.9(a)   −2.6(b)   −0.93(a)

ΔE_i^{orb} = −8.5   −8.5

ΔE_i^{orb} = −2.8(b)   −2.7(a)   −2.2(a)

ΔE_i^{orb} = −0.2   −0.2

Figure S12. Deformation density ($\Delta\rho$(r)) pictures of the pairwise orbital interactions for B$_{12}$Kr$_n$F$_{12}^{2-}$ (n = 1 and 12) along Path1 and Path2 and their associated ΔE_i^{orb} energies (ΔE^{σ} and ΔE^{π} , in kcal mol^{-1}) obtained from the EDA−NOCV at B3LYP−D3/TZ2P level of theory. The blue and red colored surfaces indicate regions with $\Delta\rho$(r) > 0 and $\Delta\rho$(r) < 0, respectively.
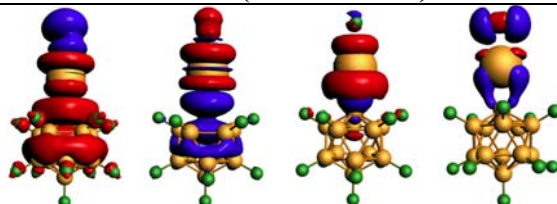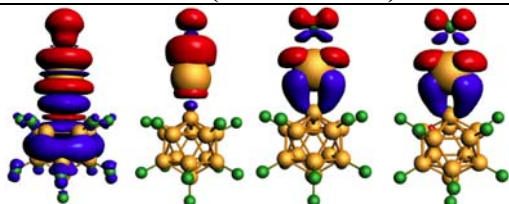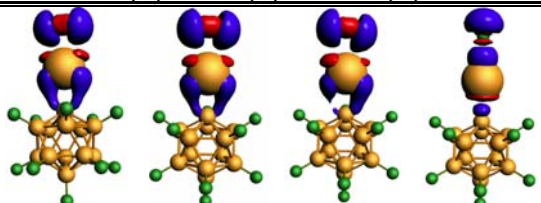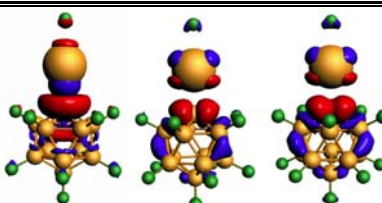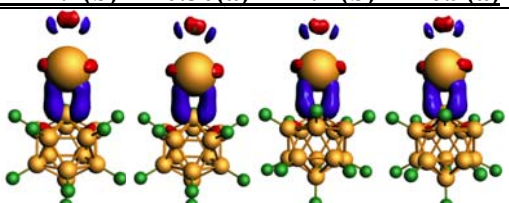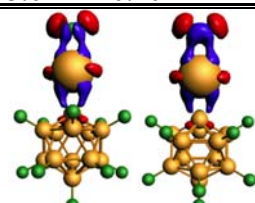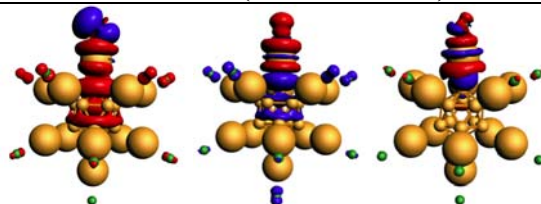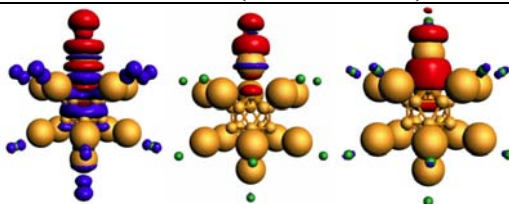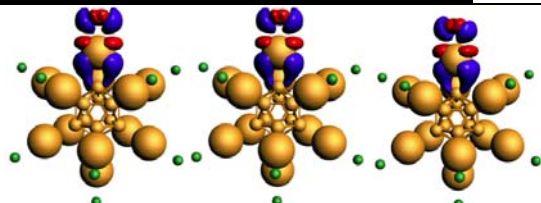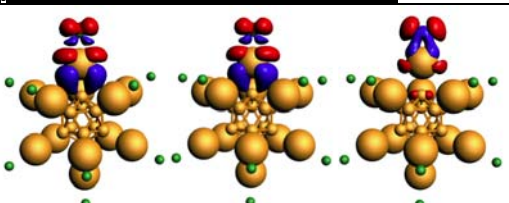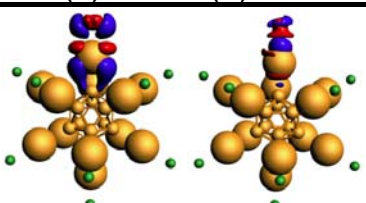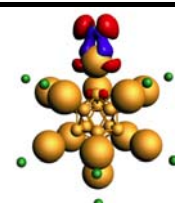
Path1 (Dianion+F+Ng) $[E^{orb} = \sum \Delta E_i^{orb}]$	Path2(Anion+F$^-$+Ng) $[E^{orb} = \sum \Delta E_i^{orb}]$
$XeB_{12}F_{12}^{2-}$ (E^{orb} =−185.1)	$XeB_{12}F_{12}^{2-}$ (E^{orb} =−134.1)

ΔE_i^{orb} = −144.0(b)   −19.1(a)   −11.0 (b)   −0.31 a | ΔE_i^{orb} = −111.3   −4.8   −5.3   −5.3

ΔE_i^{orb} = −1.1(b)   −0.30(a)   −1.1 (b)   −0.9(a) | ΔE_i^{orb} = −3.6   −0.40   −0.40

ΔE_i^{orb} = −1.0(b)   −0.7(a)   −0.7(a)   −1.0(a) | ΔE_i^{orb} =   −0.48   −0.48

$Xe_{12}B_{12}F_{12}^{2-}$ (E^{orb} =−−188.0)	$Xe_{12}B_{12}F_{12}^{2-}$ (E^{orb} =−201.8)

ΔE_i^{orb} = −116.2(b)   −36.8(a)   −13.3(b) | ΔE_i^{orb} = −161.5   −8.1   −8.0

ΔE_i^{orb} =   −2.0(a)   −2.7(b)   −1.1(a) | ΔE_i^{orb} = −9.3   −9.3   −0.5

ΔE^{orb} = −3.3(b)   −2.9(a) | ΔE_i^{orb} = −0.5

Figure S13. Deformation density ($\Delta\rho$(r)) pictures of the pairwise orbital interactions for $B_{12}Xe_nF_{12}^{2-}$ (n = 1 and 12) along Path1 and Path2 and their associated ΔE_i^{orb} energies (ΔE^σ and ΔE^π , in kcal mol^{-1}) obtained from the EDA−NOCV at B3LYP−D3/TZ2P level of theory. The blue and red colored surfaces indicate regions with $\Delta\rho$(r) > 0 and $\Delta\rho$(r) < 0, respectively.